Journal of
Materials Chemistry A

Materials for energy and sustainability

Accepted Manuscript

This article can be cited before page numbers have been issued, to do this please use: F. W. Fenta and R. Bouchal, *J. Mater. Chem. A*, 2024, DOI: 10.1039/D4TA02704C.

ROYAL SOCIETY OF CHEMISTRY

rsc.li/materials-a

View Article Online
DOI: 10.1039/D4TA02704C

Unraveling the Significance of Zinc Ratio in Water-in-Salt Electrolytes

Fekadu Wubatu Fenta and Roza Bouchal*

Max Planck Institute of Colloids and Interfaces, Am Mühlenberg 1, 14476 Potsdam, Germany.

Roza.Bouchal@mpikg.mpg.de

1. Abstract

Water-in-salt electrolytes (WISEs) have been proposed as an effective approach to suppress the side reactions related to free water activity on zinc (Zn) metal anode, thereby enhancing its electrochemical performance. While most WISEs correlate total salt concentration with water content and Zn^{2+} solvation structure, the impact of Zn ratio has been largely overlooked. In this work, we prepared a range of WISEs with varying Zn molar ratios while ensuring low water content, and scrutinized the impact on Zn nucleation behavior, Zn plating/stripping overpotential, and overall Zn metal anode stability. Our results demonstrated that the increase of Zn content in the electrolyte promotes high transference number and the 3D Zn^{2+} diffusion process – thus enhancing the Zn anode stability and reversibility. Moreover, we identified an optimized Zn molar ratio of approximately 0.5, suggesting that beyond this threshold, the impact diminishes. Our findings show that reaching the WISE region is insufficient to improve Zn metal performance; instead, an optimal concentration of Zn^{2+} ions is the determining factor. Consequently, we advocate for the optimization of Zn ratio in the future design of WISEs for high-performance Zn-ion batteries.

View Article Online
DOI: 10.1039/D4TA02704C

2. Introduction

Aqueous batteries have attracted great attention for grid-scale energy storage systems due to their low cost and high safety attributed to the use of non-flammable aqueous electrolytes.[1] Among these, aqueous Zn ion batteries (AZIBs) are promising alternatives for large-scale energy storage technologies owing to their high theoretical gravimetric (820 mAh g^{-1}) and volumetric (5855 mAh cm^{-3}) capacities, low redox potential (−0.76 V versus the standard hydrogen electrode, SHE), high abundance, and low toxicity of Zn metal anode.[2, 3] However, the undesired electrochemical reactions on the Zn anode such as hydrogen (H_2) evolution, uncontrolled dendrite growth, accumulation of dead Zn, and formation of byproducts severely affect the lifespan of AZIBs.[4]

It is widely acknowledged that the parasitic H_2 evolution occurring on the Zn anode in conventional diluted electrolytes promotes dendrite growth while also resulting in the formation of inactive Zn deposits.[4] In dilute electrolytes, the Zn^{2+} solvation shell typically consists of six water molecules, wherein the interaction between Zn^{2+} and water prompts water molecules to undergo ionization. The electric field generated by Zn^{2+} exerts a force on water molecules, facilitating electron transfer from coordinated H_2O to vacant orbitals of Zn^{2+}. This process notably weakens the O–H bonds of water molecules and promotes H_2 evolution.[5] In addition, the formation of a hydrogen bonding network among free water molecules leads to the rapid transport of protons (H^+) and hydroxide anions (OH^-) through the Grotthuss mechanism, thereby enhancing H_2 evolution.[6] These lead to continuous electrolyte consumption and pressure build-up in a cell, thus reducing the reversibility and cycling stability of Zn anode. Several approaches have been proposed to address the above-mentioned challenges by limiting water activities.[7, 8] One of the common approaches to mitigate H_2 evolution is the development of highly concentrated electrolytes also called WISEs. The higher salt-to-water ratio in WISEs does not contain sufficient water to fully coordinate the Zn^{2+} ions, thereby disrupting the original hydrogen bonding network of water, which enables the coordination of anions in the Zn^{2+} solvation structure.[9] Thus, the partial replacement of water by anions in the Zn^{2+} solvation structure are

View Article Online
DOI: 10.1039/D4TA02704C

assumed to mitigate the H_2 evolution upon Zn electrodeposition, improving the cycling stability and Columbic efficiencies of Zn metal batteries. For example, Zhang *et al* reported dendrite free Zn metal anode using 30 m $ZnCl_2$ electrolyte (m = mol of salt/1 Kg of sovent), which improved the Zn plating/stripping reversibility.[10] Yang *et al* showed that Zn reduction occurs before H_2 evolution as the concentration of $ZnCl_2$ increases due to the high overpotential against H_2 evolution on Zn metal.[11] This expands the voltage gap between Zn reduction and H_2 evolution that helps to minimize parasitic reactions. On the other hand, due to the limited solubility of most Zn salts in water, the reported WISEs are combined with another salt such as lithium bistrifluoromethanesulfonimide (LiTFSI) or potassium acetate (KAc) and others e.g. 1 m $Zn(TFSI)_2$ + 20 m LiTFSI,[9] 1 m $Zn(Ac)_2$ +31 m KAc,[12] and 0.5 m $Zn(ClO_4)_2$ + 18 m $NaClO_4$.[13] This results in a very low Zn salt content, accounting for only 2-8 % of the total electrolyte concentration, thus causing a high overpotential above 0.1 V. The latter leads to kinetic limitations, heat generation, and uneven distribution of electrode active material, resulting in dendrite formation. However, a high Zn cation density near the electrode interface is necessary to counterbalance the poor ionic conductivity in WISEs, which otherwise fosters dendrite formation and slows down electrode kinetics. Elevated viscosity also contributes to high overpotential, known as concentration polarization, occurring when the rate of mass transport of reactants to/from the electrode restricts current to flow. Despite numerous reports correlating electrolyte concentrations with water quantity and Zn^{2+} solvation structure, the impact of Zn content in WISEs on Zn anode performance has been largely overlooked. Hence, it is crucial to comprehend to what extent the elevation of salt concentration to achieve the WISE region is significant in relation to the Zn molar ratio.

Herein, we prepared WISEs based on Brønsted-Lowry concept by mixing Zn chloride ($ZnCl_2$) and lithium acetate (LiAc).[14] This concept allows us to obtain various Zn molar ratios while maintaining the WISE region with a very low water content. Thus, we prepared four WISEs by varying the $ZnCl_2$ molar ratio in $ZnCl_2$/LiAc mixtures (0.2, 0.5, 0.8, and 1) and compared with the widely studied WISE (1m $Zn(Ac)_2$ + 31 m KAc) by Chen *et al*.[12] Furthermore, we examined how the total salt and Zn^{2+} concentrations in WISEs affect the Zn nucleation behavior, Zn^{2+} transference number, and Zn plating/stripping efficiency. Moreover, to establish a correlation

View Article Online
DOI: 10.1039/D4TA02704C

between the Zn ratio and water concentration, we examined a diluted version of 0.5 ratio electrolyte and compared it with the recently reported WISE-like solution by Vazquez *et al* composed of $Zn(Ac)_2$ and KAc salts.[15] Our primary objective in this study is to comprehend the influence of the Zn^{2+} molar ratio in WISEs on Zn anode cycling stability, supplemented by an analysis of the impact of water concentration. This study will help to target the future design of Zn aqueous electrolytes by considering both the Zn molar ratio and the amount of water, which is an efficient strategy to find a balance between high energy and high power densities.

3. Results and discussion

3.1. Electrolyte formulation and solvation structure

To demonstrate the correlation between Zn molar ratio and Zn anode stability, a series of WISEs was prepared by mixing $ZnCl_2$ and LiAc salts at room temperature. $ZnCl_2$ is used because of its high solubility and dissociation constant. LiAc is used as a supporting salt to achieve the WISE region while varying the $ZnCl_2$ salt ratio. In addition, the lithium cation (Li^+) is a weak acid which could not increase the Brønsted-Lewis acidity of the electrolyte. In such WISEs, the molar ratio of $ZnCl_2$ and LiAc in $(ZnCl_2)_x(LiAc)_{1-x}$ /$(H_2O)_n$ mixtures are varied, where "x" is the molar ratio of $ZnCl_2$ (x= 0, 0.2, 0.5, 0.8, 1), whereas "n" is the water content per total salt. After here, **xZn** is used for simplicity to represent the WISEs. The measured Liquidus line in **Fig. S1** shows that the solubility of $(ZnCl_2)_x(LiAc)_{1-x}$ /$(H_2O)_n$ slightly increases as the $ZnCl_2$ increases, where the water content varies from n = 2.38 to n = 1.77. Note that, the solubility limit changes with the salts ratio and obtaining the exact same salt concentrations for all electrolytes is not possible. The corresponding total salt concentrations are 23, 27, 28, and 31 m while that of Zn^{2+} concentrations are 5, 14, 25, and 31 m for **0.2**, **0.5**, **0.8**, and **1Zn** electrolytes, respectively. The pH value continuously decreases from basic to highly acidic as the Zn molar ratio increases from **0.03** to **1,** *see* **Table S1**. This increase in acidity is attributed to the complex Zn solvation structures, primarily consisting of $(Zn(H_2O)Cl_4)^{2-}$ and $Zn(H_2O)_6^{2+}$ species.[16, 17] Hydrogen ions are released from the coordination shell of the octahedral hydrated Zn complex, leading to the increased acidity of the solution. This indicates the number of hydration molecules directly affects the pH of the solution. The lower hydration levels significantly strengthen the proton activity in the electrolyte thus resulting in lower acidity. According to the Pourbaix diagram, when pH < 4.0, Zn has a high

View Article Online
DOI: 10.1039/D4TA02704C

solubility and can be easily dissolved as Zn^{2+}.[18] The $(ZnCl_2)_x(LiAc)_{1-x}/(H_2O)_n$ WISEs were compared with previously reported Zn-deficient WISE composed of 1 m $Zn(Ac)_2$ + 31 m KAc.[12] This electrolyte was selected because it is a benchmark for WISE having high total salt concentration (32 m) and a very low mole of Zn^{2+} (**0.03**), abbreviated as **0.03Zn** hereafter. Thus, in total, we prepared five WISEs with Zn molar ratios ranging from **0.03** to **1**, as demonstrated in **Fig. S1**.

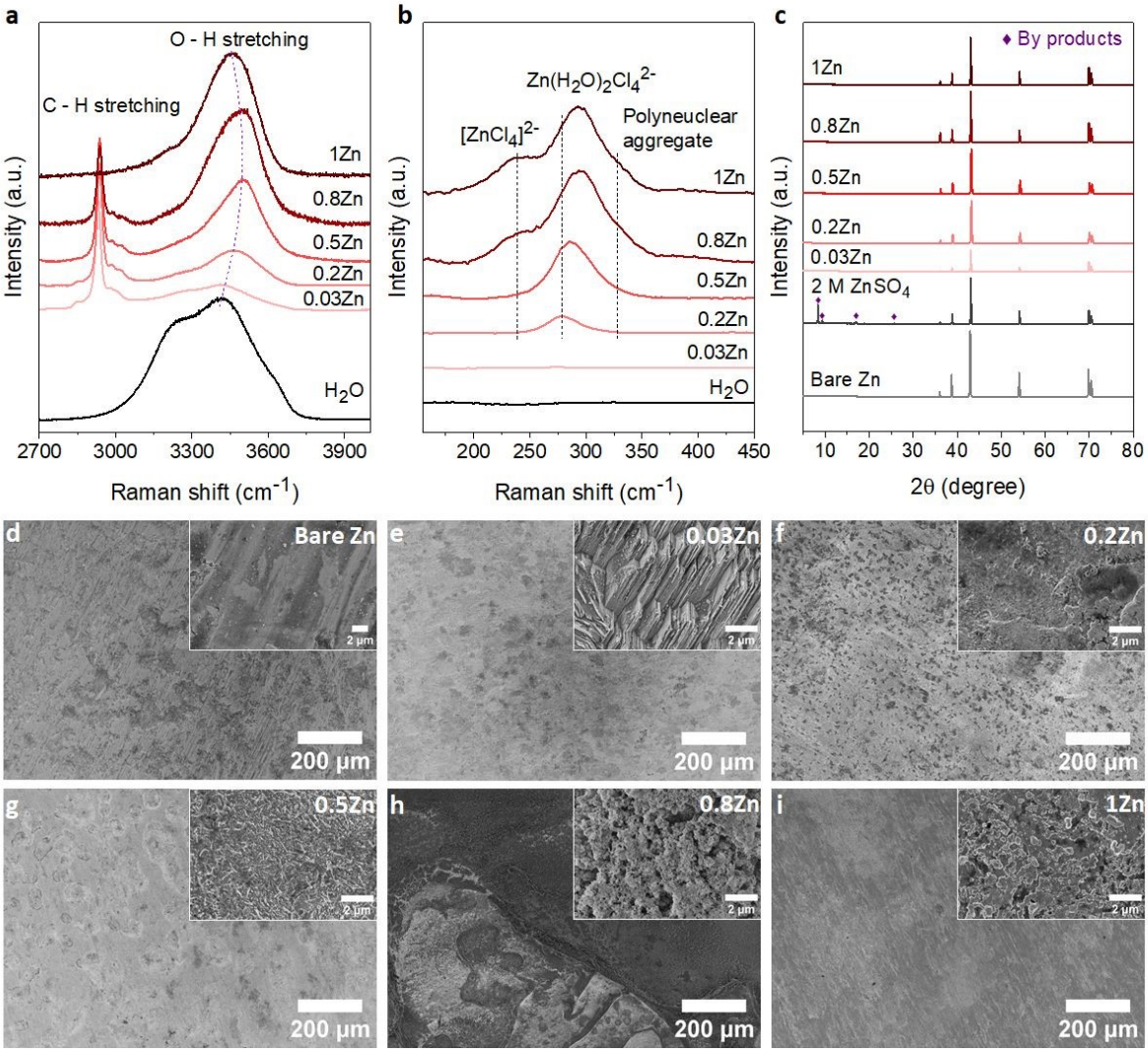

Figure 1: Electrolyte structure and Zn foil stability: (a) and (b) Raman spectra of WISEs corresponding to water region and Zn coordination, respectively. (c) XRD patterns of the Zn foils before and after immersing in different WISEs for 10 days at room temperature, compared with diluted 2M $ZnSO_4$. SEM images of (d) bare Zn foils and soaked Zn foil in (e) 0.03Zn, (f) 0.2Zn, (g) 0.5Zn, (h) 0.8Zn, and (i) 1Zn WISEs.

Raman spectroscopy was conducted to study the evolution of H-bonds, Zn^{2+} coordination, and cation-anion interactions in the prepared WISEs. **Figure 1a** shows the O-H stretching Raman

View Article Online
DOI: 10.1039/D4TA02704C

spectra for water in the high-frequency region (2700 – 3900 cm^{-1}). The broad peak of the water region narrows and initially shifts to higher frequencies and then to the lower frequencies as the $ZnCl_2$ molar ratio increases. It is important to note that the water environment is not directly influenced by the amount of Zn molar ratio, but rather by the electrolyte composition and concentration. Notably, an important blue shift of the O-H stretching mode is observed in the **0.5Zn** electrolyte. This observation suggests that Ac anions influence the strengthening of O-H bonds in water molecules by interacting with the oxygen atoms of Ac and the hydrogen atoms of water. However, compared to the **0.5Zn** electrolyte, water region shifts to the lower frequencies for **0.8** and **1Zn** electrolytes, indicating the weakening of O-H bonds probably due to the interaction of water with Zn^{2+} and/or Li^+ ions. Furthermore, the peaks related to the water region were deconvoluted into three sub-bands corresponding to non H-bond (coordinated water), weak H-bond, and strong H-bond, as shown in **Fig. S2**.[19] The results show difference in H-bonding enviroments depending on the ratio of LiAc and $ZnCl_2$ salts in each electrolyte, making difficult to obtain a correlation between salt ratios and the H-bonding enviroments of water. The above results indicate that the changing of molar ratios of $ZnCl_2$ and LiAc influence the interaction between water molecules and Zn^{2+}, Ac, and Li^+ ions. This in turn, affects the position and intensity of O-H stretching mode of water molecules in the each electrolyte.

Figure 1b illustrates the Zn^{2+} coordination in the low-frequency region (~140 - 500 cm^{-1}), resulting from the interaction of Zn^{2+} with H_2O molecules and Cl^- ions. As expected, no peaks corresponding to **0.03Zn** electrolyte are observed in this region due to the absence of Cl^- ions. The peak at 278 cm^{-1} in **0.2Zn** electrolyte is assigned to $Zn(H_2O)Cl_4^{2-}$ complex. The latter shows an increase in intensity and shifting to higher frequencies with the rising Zn molar ratio (**Fig. 1b**). The additional peaks observed at 240 and 328 cm^{-1}, in **0.8** and **1Zn** electroytes, are attributed to the $[ZnCl_4]^{2-}$ complex and Zn-Cl polynuclear aggregate, respectively, according to previously reported works.[14]

Furthermore, the coordination of Zn^{2+} with Ac anions can be examined in the 400-1450 cm^{-1}. For a better correlation, the reported WISEs were compared with saturated LiAc (sat. LiAc) solution. The in-plane O-C-O rocking vibration at 476 cm^{-1} in sat. LiAc completely shifts to the higher frequencies upon increasing $ZnCl_2$ ratio (**Fig. S3a**), indicating the interaction of Zn^{2+} with Ac

View Article Online
DOI: 10.1039/D4TA02704C

anions.[20] Similar to the peaks related to COO bending at 656 cm^{-1}, the C-C stretching at 932 cm^{-1}, and C=O stretching at 1419 cm^{-1}, which all undergo a blue shift with $ZnCl_2$ concentration in the prepared WISEs. The C=O stretching peak at 1419 cm^{-1} split into two for **0.5** and **0.8Zn** electrolytes (**Fig. S3b**), suggesting simultaneous coordination of Ac to Li^+ and Zn^{2+}.[20] These results indicate the preference of Ac anion to interact with Zn^{2+} rather than to Li^+. Finally, regarding **0.03Zn** electrolyte, all the peaks show a red shift in comparison to all electrolytes including sat. LiAc. These results indicates the dominant interaction of K^+ to Ac anions due to low amount of Zn^{2+} cations in **0.03Zn** electrolytes.

3.2. Stability of Zn foil in different WISEs

According to Raman results, water molecules interact with anions and cations present in each WISEs in distinct ways. Prior to electrochemical tests, immersion experiments were conducted to assess the impact of these WISEs on the thermodynamic stability of Zn metal anodes. For this, a Zn foil was immersed in the prepared WISEs for a period of 10 days, subsequently rinsed with deionized water, and dried under vacuum. The surface change of Zn foil before and after soaking were then analyzed using X-ray powder diffraction (XRD) and scanning electron microscopy (SEM). For comparison, the XRD pattern of the Zn foils immersed in WISEs were compared with those immersed in 2M $ZnSO_4$ and 1 m $ZnCl_2$ diluted electrolytes. As expected the 2M $ZnSO_4$ shows a distinct byproduct formation, which is identified as $Zn_4SO_4(OH)_6{\cdot}5H_2O$ byproduct ((*see* **Fig. 1c)**,[21] while only one characteristic byproduct peak is observed in 1 m $ZnCl_2$ (**Fig. S4**).[22] In contrast, no XRD patterns of byproducts are observed on the Zn foil soaked in different WISEs. This suggests that byproduct formation is influenced by both the type of Zn salt and concentration. In addition, SEM images are performed to analyze the surface of Zn metal in relation to the Zn molar ratio (**Fig. 1d-i**). The bare Zn foil has a rough and uneven surface as indicated in **Fig. 1d**, which could have been caused by the manufacturing process. In **Fig. 1e**, the electrode displays surface etching in structured form parallel to each other in **0.03Zn** electrolyte. Dark spots and white small mossy particles cover the Zn surface in **0.2** and **0.5Zn** electrolytes (**Fig. 1f-g**), while the Zn surface in **0.8** and **1Zn** (**Fig. 1h-i**) displays pitting spots and particles formation, especially in **0.8Zn** electrolyte. The latter is related to corrosion byproduct due to increased acidity. Overall, in all WISEs clear corrosion is observed only at higher magnification except for **0.8Zn**. The immersion test reveals

View Article Online
DOI: 10.1039/D4TA02704C

that the side reactions generated from the direct interaction between the Zn anode and WISEs are lower in comparison to diluted electrolytes.

3.3. Zn electrodeposition behavior

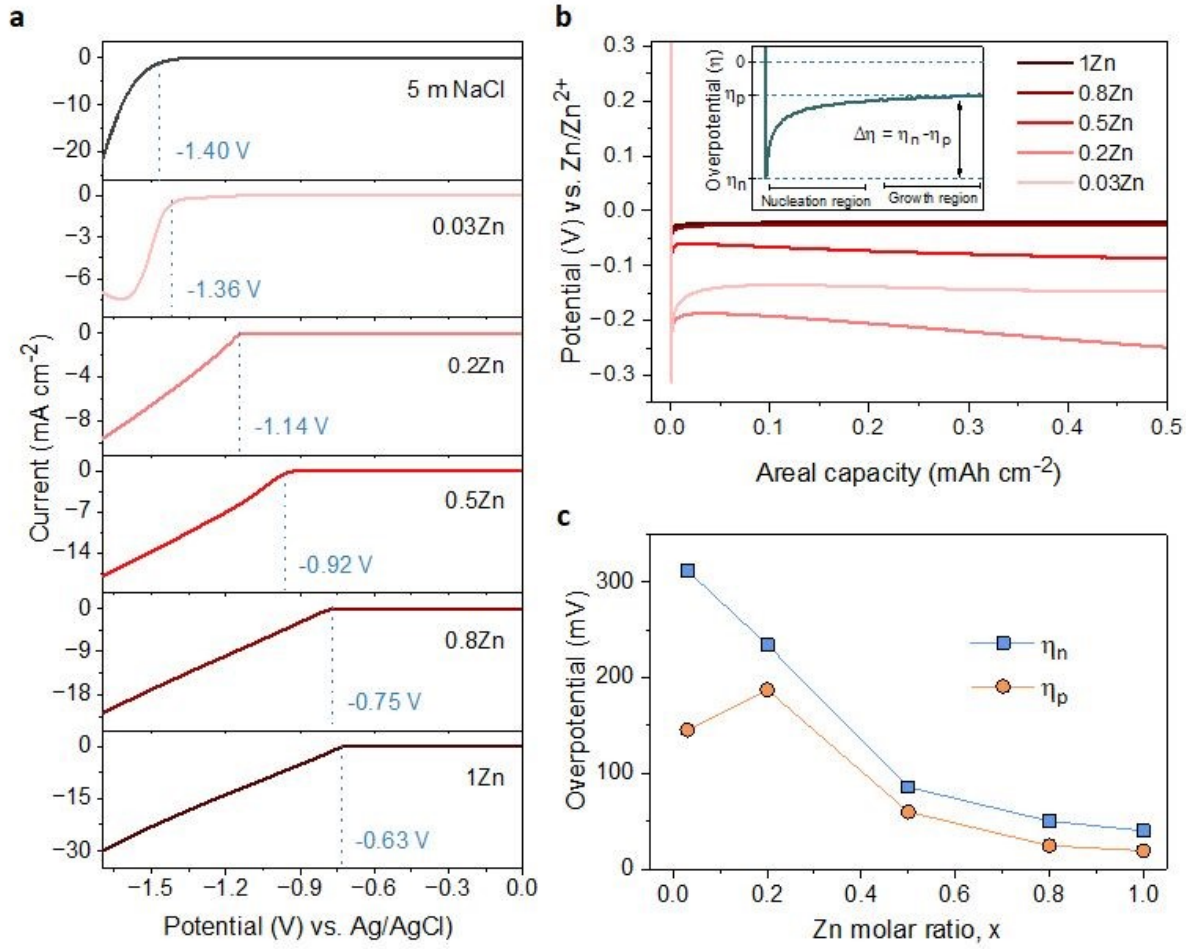

Figure 2: H_2 evolution and Zn deposition potentials in different WISEs. (a) LSV profiles of different electrolytes at 10 mV s^{-1} using a three-electrode system on Ti substrate. (b) Galvanostatic Zn electrodeposition on Ti in Zn‖Ti half cells at 1 mA cm^{-2} and 0.5 mAh cm^{-2} using different WISEs. Inset: Schematic illustration showing nucleation overpotential (η_n), plateau overpotential (η_p), and the change in overpotential ($\Delta\eta$). (c) The corresponding change in η_n, η_p, and $\Delta\eta$ with Zn molar ratio.

To examine the effect of Zn molar ratio on H_2 evolution and Zn reduction potential in different WISEs during electrodeposition processes, linear sweep voltammetry (LSV) measurements were conducted. Indeed, it is common that in Zn^{2+} containing aqueous electrolytes, the H_2 evolution occurs during Zn electrodeposition at similar reduction potential.[23] As a result, to discriminate the Zn reduction from H_2 evolution, the WISEs were compared to a Zn-free electrolyte, here 5 m NaCl solution. The experiments were performed using titanium foil (Ti) as working, Ag/AgCl as

View Article Online
DOI: 10.1039/D4TA02704C

reference, and platinum as counter electrodes at a scan rate of 10 mV·s^{-1}. The 5 m NaCl solution reveals a reduction potential occurring at –1.4 V (**Fig 2a**), indicative of H_2 evolution, given the absence of Zn^{2+} in the NaCl solution. In contrast, the onset reduction potential of **0.03Zn** electrolyte is –1.36 V, which corresponds to Zn^{2+} reduction voltage – given that the water content is very low. As the Zn ratio increases from **0.2** to **1**, reduction potentials of –1.14, –0.92, –0.75, and –0.63 V are observed. Moreover, we conducted additional LSV experiments on a glassy carbon (GC) substrate using a three-electrode system at scan rates of both 10 and 1 mV s^{-1} (**Fig. S5a** and **b**, respectively). The resulting reduction potentials in each electrolyte were similar to those obtained with a Ti substrate, indicating similar kinetics limitations using different substrates and scan rates. This result is consistent with previous findings in the literature by using different $ZnCl_2$ concentration ranging from 1 to 30 m.[11, 24] Therefore, the positive Zn reduction potential observed with increasing Zn molar ratios is primary attributed to the increased Zn^{2+} activity due to the lower acidity of the electrolyte, according to the Nernst equation below:

$$E = E^{\circ} + \frac{RT}{2F} ln\alpha_{[zn^{2+}]} \quad (1)$$

Where E is the reduction potential, E° is the the standard reduction potential, R is the universal gas constant, T is the temperature in kelvin, F is the Faraday's constant, and α is the activity of Zn^{2+} ions. In addition, the LSV of the **0.03Zn** electrolyte with a pH of 10.9 was compared to a **31 m KAc** solution without Zn salt displaying a similar pH of 11.4, as shown in **Fig. S6**. The reduction potential increased from –1.60 V and –1.62 V in **31 m KAc** to –1.37 and –1.33 V in **0.03Zn** on Ti and GC at 10 and 1 mV s^{-1}, respectively. This increase in onset potential suggests that Zn deposition occurs before H_2 evolution in the **0.03Zn** electrolyte. Similar findings were reported by Daniel *et al* in an electrolyte containing 10 m KAc + 0.5 m ZnAc.[25] As a conclusion, the Zn deposition potential increases with Zn molar ratio, while the H_2 evolution potential remains constant, expanding the voltage gap between H_2 evolution and Zn deposition. The large voltage gap minimizes H_2 evolution and other side reactions, thereby improving Zn anode performance.[26]

The suppression of H_2 evolution may not consistentely indicate dendrite free Zn deposition. Additional insights into the effect of Zn^{2+} concentration in the electrolyte on Zn deposition are necessary. It is widely acknowledged that the final morphology of deposited metal relies on the

View Article Online
DOI: 10.1039/D4TA02704C

initial nucleation behavior.[27] Understanding the mechanism of nucleation behavior is crucial for addressing the formation of Zn dendrites which can be assessed through nucleation overpotential (η_n), driving the nucleation of Zn embryos.[28] A smaller nucleation overpotential implies a lower energy barrier for initiating the Zn nucleation process, thereby facilitating uniform Zn nucleation site formation .[29, 30] Hence, cyclic voltammetry (CV) experiments were conducted in a three-electrode system on Ti foil and GC substrates as the working electrode, platinum wire as the counter electrode, and Ag/AgCl as the reference electrode, with a scan rate of 10 mV S^{-1} within a potential range of -1.7 to 1.0 V. The CV curves (**Fig. S7**) for both electrodes exhibit similar Zn deposition/dissolution behavior across various WISEs, indicating reversibility and the absence of new redox reactions. However, the redox potential shifts to the right with increasing Zn ratio due to higher Zn^{2+} activity at greater Zn^{2+} concentrations. Additionally, η_n can be calculated from the potential difference between point (A), where Zn^{2+} ions begin to reduce, and the crossover at point (A') formed during the right potential sweep as depicted in **Fig. S8**. The η_n measured using Ti electrode decreases as the Zn^{2+} concentration increases: 103, 65, 43, and 37 mV corresponding to **0.03**, **0.2**, **0.5**, **0.8**, and **1Zn** electrolytes, respectively. However, with the exception of the **0.5Zn** electrolyte, no clear potential difference between A and A' was observed, which cannot be explained.

Furthermore, the galvanostatic Zn deposition process is commonly employed not only to determine η_n but also to assess another crucial parameter linked to growth, known as plateau overpotential (η_p). η_n represents the magnitude of the potential spike at the onset of Zn deposition, while η_p denotes the potential at the plateau following nucleation (*see* **Fig. 2b**).[31] Additionally, the overpotential difference ($\Delta\eta$) is defined as the gap between η_n and η_p. The η_n values are notably larger than the η_p values in all electrolytes due to the higher energy barrier involved in forming a stable Zn atomic cluster (embryo) compared to adding a Zn atom onto existing Zn nuclei (**Fig. 2c**), indicating that the electrodeposition of Zn follows the instantaneous nucleation process.[32] For instance, the η_n decreases as the Zn molar ratio increases: 311, 234, 86, 50, and 40 mV for **0.03**, **0.2**, **0.5**, **0.8** and **1Zn** electrolyts, respectively (**Fig. S9**). Simultaneously, the η_p values are 145, 187, 60, 25, and 19 corrosponding to **0.03**, **0.2**, **0.5**, **0.8** and **1Zn** electrolytes, respectively. Similarly, $\Delta\eta$ decreases with Zn molar ratio; 166, 47, 26, 25, and 19 mV

View Article Online
DOI: 10.1039/D4TA02704C

256 for **0.03**, **0.2**, **0.5**, **0.8**, and **1Zn** electrolytes, respectively. The results show that the high Zn^{2+}
257 concentration reduces the energy barrier for Zn nucleation and growth, likely due to reduced
258 kinetics/diffusion resistance - promoting homogeneous Zn deposition.[33,30]
259

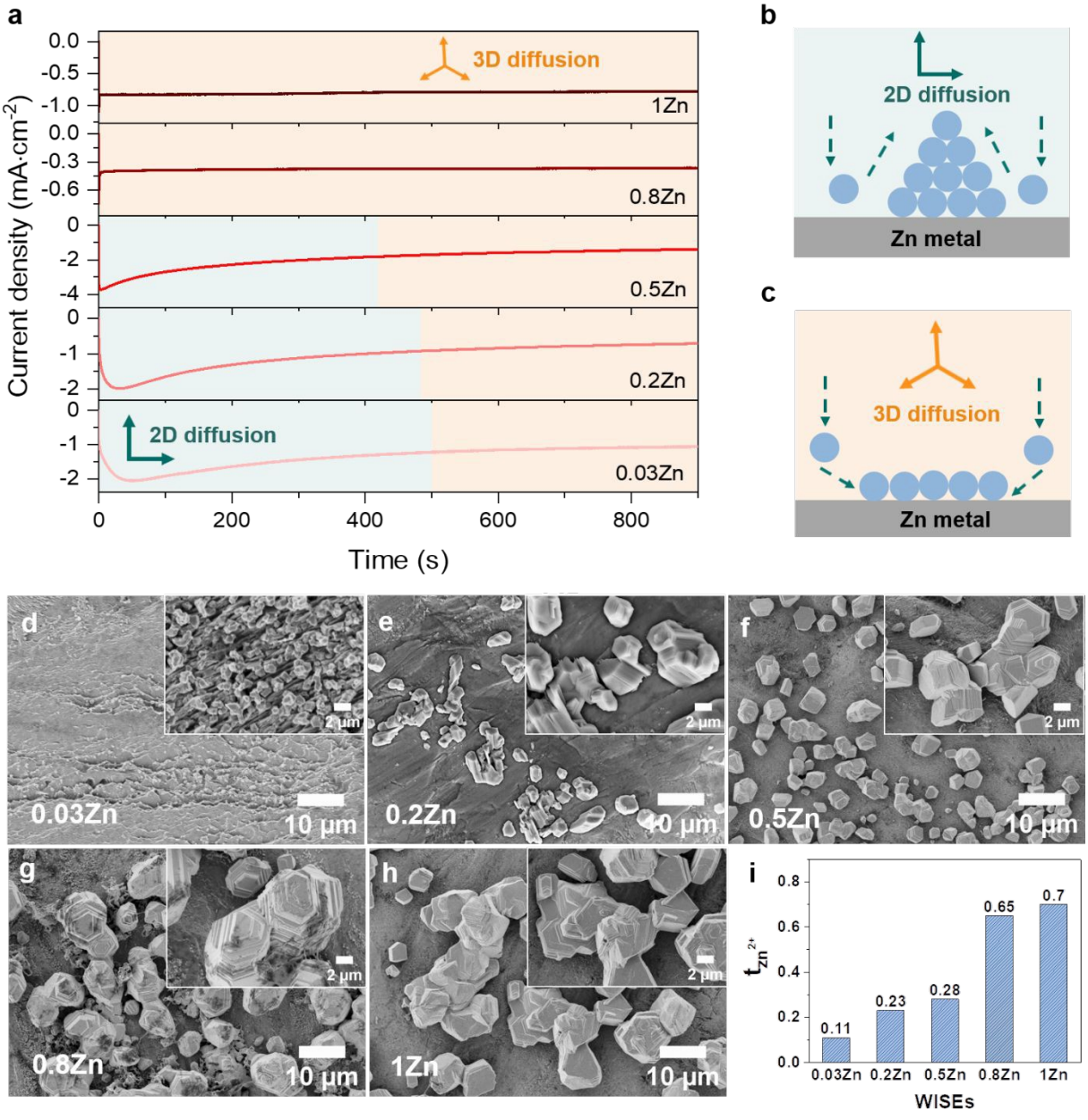

260

261 **Figure 3: Zn diffusion process and the corresponding ions mobility in different WISEs.** (a)
262 Chronoamperograms (CAs) of Zn deposition at an applied potential of -150 mV for 900 s. Insets: 2D (left)
263 and 3D (right) diffusion for 0.03, 0.2, and 0.5Zn electrolytes; 3D diffusion for 0.8 and 1Zn electrolytes.
264 Schematics showing (b) 2D and (c) 3D diffusion processes. The corresponding SEM images of deposited

View Article Online
DOI: 10.1039/D4TA02704C

Zn in (d) 0.03, (e) 0.2, (f) 0.5, (g) 0.8, and (h) 1Zn electrolytes. (i) The transference number in different electrolytes.

The Zn nucleation and growth behavior were further analyzed on Zn metal by chronoamperometry (CA) experiment at a fixed potential of -150 mV for 30 min using Zn‖Zn symmetric cells. The fluctuation of current transients can indicate a change in nucleation processes and surface morphology.[27] As depicted in **Fig. 3a**, the current density exhibits a steady rise over 50, 30, and 5 seconds in **0.03**, **0.2**, and **0.5Zn** electrolytes, respectively, followed by a plateau, suggesting an initial phase of uncontrolled 2D diffusion transitioning into 3D diffusion. During 2D diffusion process, Zn atom diffuse laterally to get the energetically favorable sites for deposition,[34] which brings inhomogeneous nucleation on the Zn metal surface and accelerates dendrite growth (**Fig. 3b**). In contrast, in **0.8** and **1Zn** electrolytes, a constant current density was observed from the beginning referring to as 3D diffusion process (**Fig 3b**). This implies that the Zn^{2+} ions are homogeneously deposited on the Zn electrode surface as the concentration of Zn^{2+} ions increases. These results are supported by the SEM images of the corresponding deposited Zn in **Fig. 3d-g**. The electrolyte with the lowest Zn ratio (**0.03Zn**) shows a very small and distributed Zn deposition particles (**Fig. 3d**). As the Zn molar ratio increases, the size of Zn nuclei grows and interconnect each other to form a dense and compact Zn deposition (**Fig. 3e-h**), indicating 3D deposition process. The results from CA and the corresponding SEM images consistent with the η_n results in **Fig. 3c**, demonstrating that a higher Zn molar ratio contributes to uniform and 3D Zn^{2+} deposition processes. This suppresses dendrite formation by enhancing nucleation sites.[29]

Furthermore, the cationic mobility in the bulk electrolyte is examined through transference number which represents the ionic current carried by cations only. The Zn^{2+} transference number (t_{Zn}^{2+}) was measured using the steady-current method, employing constant applied potential to generate current-time(I-t) transient using Zn‖Zn symmetric cells (**Fig. S10)**.[35, 36] The t_{Zn}^{2+} for **0.03**, **0.2**, **0.5**, **0.8**, **1Zn** WISEs are calculated to be 0.11, 0.23, 0.28, 0.65, and 0.70, respectively. This indicates that electrolytes containing high Zn^{2+} concentrations exhibit higher t_{Zn}^{2+} compared to those with lower concentrations, suggesting that Zn^{2+} ions serve as the primary mobile ions to reduce polarization.[37] This explains why the η decreases when the Zn^{2+} ions concentration

View Article Online
DOI: 10.1039/D4TA02704C

increases, as demonstrated in **Fig. 2b-c**. Moreover, the high t_{Zn}^{2+} effectively enhances the anode's electrochemical performance, and significant t_{Zn}^{2+} can mitigate dendrite growth.[19] Additionally, the transport properties of WISEs including ionic conductivity, viscosity and ionicity were further characterized and compared to t_{Zn}^{2+}. The viscosity values for **0.03**, **0.2**, **0.5**, **0.8**, and **1Zn** electrolytes are 48, 537, 265, 317, and 465 mPa·s, respectively, while the corresponding ionic conductivity values are 29, 4, 8, 5, and 6 mS cm^{-1}, respectively (**Table S1**). All WISEs display low ionic conductivity and high viscosity except **0.03Zn** electrolyte which displays an opposite trend (**Fig. S11a**). The later may be attributed to the high solubility of KAc and the lower acidity of K^+ which results in lower ion pairing and allows for greater ion mobility, further enhancing ionic conductivity. These findings confirm that the increase in the t_{Zn}^{2+} is directly related to the Zn molar ratio. Furthermore, a Walden plot was used to investigate the relationship between the ionic conductivity and viscosity which reflects the ionicity of the electrolytes. **Fig. S11b** indicates no direct correlation between the Zn molar ratio and ionicity, which is expected. Electrolytes with Zn molar ratios of **0.03**, **0.2**, and **0.5Zn** exhibit a higher degree of dissociation, with **0.03** and **0.2Zn** displaying super ionicity as they are located above the KCl ideal line. In contrast, the other electrolytes, including **0.8**, **1Zn**, and diluted **0.5Zn**, show a slightly lower degree of ionicity, around 90%.

View Article Online
DOI: 10.1039/D4TA02704C

3.4. Zn anode cycling stability

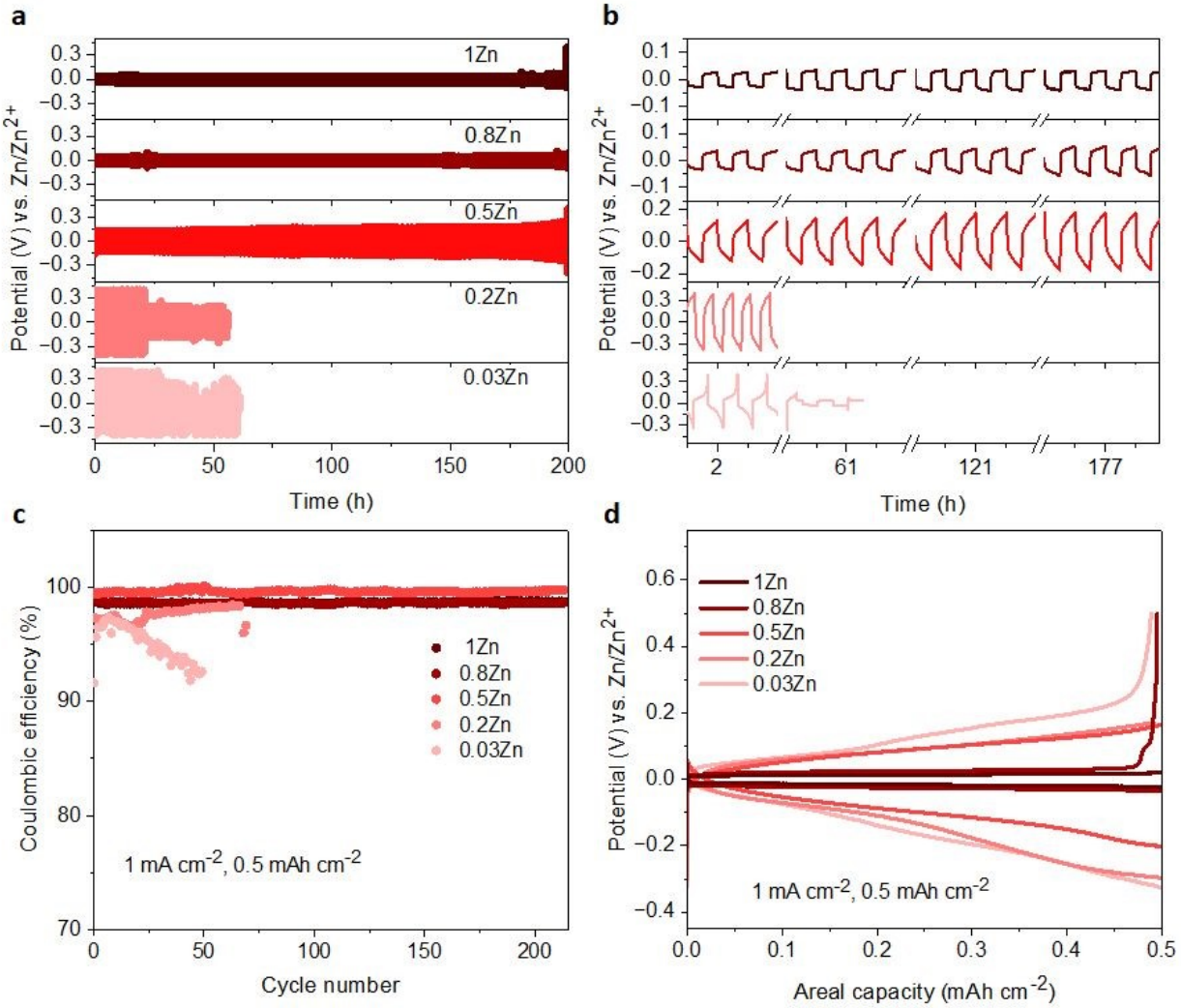

Figure 4: Zn plating/stripping stability. Potential profiles for Zn‖Zn cells conducted in 0.3, 0.2, 0.5, 0.8, and 1Zn electrolytes at current densities of (a) 2 mA cm^{-2} with 0.5 mAh cm^{-2} and (b) the corresponding overpotentials at different cycles. (c) CE of Zn plating/stripping on Cu substrate in different electrolytes at 1 mA cm^{-2} and 0.5 mAh cm^{-2} current and capacity densities, respectively. (d) The corresponding potential profiles at 40th cycle.

The Zn plating/stripping stability was evaluated in Zn‖Zn symmetrical cells under current densities of 1 and 2 mA cm^{-2}, maintaining an areal capacity of 0.5 mAh cm^{-2}. The cycle lifespans of cells in **0.03Zn**, **0.2Zn**, **0.5Zn**, **0.8Zn**, and **1Zn** WISEs at 1 mA cm^{-2} are 85, 55, 300, 350, and 500 hours, respectively (**Fig. S12a**). The results indicate an improved cycling stability upon increasing Zn ratio except for **0.2Zn** electrolyte which exhibits slightly shorter cycle lifespan compared to **0.03Zn** electrolyte. In addition, lower plating-stripping overpotentials are observed for

View Article Online
DOI: 10.1039/D4TA02704C

electrolytes with higher Zn molar ratios from ~0.35 V in **0.03** to ~0.1 V in **1Zn** (**Fig. S12b).** Increasing the current density to 2 mA cm^{-2} with the same areal capacity of 0.5 mAh cm^{-2} results in cells failing after 25 hours of cycling in **0.03** and **0.2Zn** electrolytes, while cells in **0.5Zn**, **0.8Zn**, and **1Zn** electrolytes sustains 200 hours of cycling (**Fig. 4a**). The corresponding overpotentials in **0.03Zn** and **0.2Zn** electrolytes are around 0.7 V, while in **0.5Zn**, **0.8Zn**, and **1Zn** electrolytes, overpotentials slightly decrease with increasing Zn ratios to 0.3 V for **0.5Zn** and 0.18 V for **0.8Zn** and **1Zn** electrolytes (**Fig. 4b**). The overpotential in **0.5Zn** electrolyte slighlty increased with cycling time, while for **0.8Zn** and **1Zn**, remains constant. The decrease in overpotential as the Zn molar ratio increases underscores the role of Zn^{2+} mobility in reducing overpotential. Deviation of overpotential from the ideal value of 0 V vs Zn/Zn^{2+} during Zn plating/stripping process suggests contributions from several factors, including H_2 evolution, corrosion byproducts such as $Zn(OH)_2$ and ZnO, or low transference number.[23, 27] As all electrolytes exhibit reduced water content, suggesting suppression of H_2 evolution during Zn plating/stripping. Consequently, Zn^{2+} concentration becomes a determining factor in compensating for Zn loss attributed to the formation of $Zn(OH)_2$ and ZnO. Therefore, achieving an optimal Zn^{2+} concentration in WISEs becomes crucial for enhancing the stability of Zn anodes. Hence, electrolytes with **0.5Zn**, **0.8Zn**, and **1Zn** compositions demonstrate favorable reversibility and plating kinetics of Zn.

Moreover, the Coulombic efficiency (CE) serves as a pivotal metric for assessing the reversibility of the Zn anode. To mitigate the influence of Zn^{2+} ions originating from the Zn electrode, CE assessments should be conducted using a different substrate. Consequently, the CE of Zn plating/stripping across various WISEs was evaluated employing Zn‖Cu at a current density of 1 mA cm^{-2} and a capacity of 0.5 mAh cm^{-2}, as shown in **Fig. 4c**. An initial CEs of 91.6, 97.3, 99.4, 99.1, and 98.7% are obtained in **0.03**, **0.2**, **0.5**, **0.8** and **1Zn** electrolytes, respectively. The cells using **0.03** and **0.2Zn** electrolytes fail after 50 and 70 cycles with an average CE of 94.9 and 96.9%, respectively. Low CE values are observed in Zn-deficient electrolytes during Zn plating/stripping in contrast to the cells employing **0.5**, **0.8**, and **1Zn** electrolytes demonstrating a stable reversibility with an average CEs of 99.6, 98.6, and 98.6 % after 214 cycles, respectively. Remarkably, the CE value generally increases with rising Zn^{2+} concentration, except for the 0.5Zn electrolyte, where the highest CE is observed. However, no significant differences are observed

View Article Online
DOI: 10.1039/D4TA02704C

among CE values starting from a **0.5Zn** ratio. Furthermore, a similar trend in CE is shown using Ti as substrate in Zn‖Ti half-cells (**Fig. S13**) at 1 mA cm^{-2} and 0.5 mAh cm^{-2}. Short cycling life is obtained in **0.03Zn** and **0.2Zn** electrolytes, however, as the concentration of Zn^{2+} increases the cell runs for 100, 180, and 260 cycles with (>96%) CE in **0.5Zn**, **0.8Zn**, and **1Zn** electrolytes, respectively.

Furthermore, **Fig. 4d** and **Fig. S14** display the potential profiles in Zn‖Cu half-cells which demonstrate a lower and stable plateau overpotentials as the Zn ratio increases. A higher overpotential of 183 mV is obtained in **0.03Zn** electrolyte, whereas an overpotentials of 164, 135, 47 and 30 mV are obtained in **0.2**, **0.5**, **0.8**, and **1Zn** electrolytes after 40^{th} cycles, respectively. The above results show that the Zn molar ratio of **0.5** and above provide better Zn anode performance compared with **0.03** and **0.2**. Thus, suggesting an optimum amount of Zn^{2+} concentration should be present in the electrolyte rather than simply increasing the supporting salt to achieve WISE region. This in turn reduces the interfacial resistance related with the supporting salt, which is manifested by the lower overpotentials and polarization for Zn plating/stripping. According to these results, Zn molar ratios less than **0.5** have a significant influence, whereas those greater than **0.5** have less influence, indicating the need for an optimal Zn^{2+} concentration to achieve enhanced Zn plating/stripping in WISEs.

3.5. Zn surface composition after cycling

To further examine the influence of Zn molar ratio on facilitating uniform Zn^{2+} deposition, the surface morphology of Zn and the resulting interphase following cycling were analysed employing SEM and X-ray photoelectron spectroscopy (XPS) techniques.

View Article Online
DOI: 10.1039/D4TA02704C

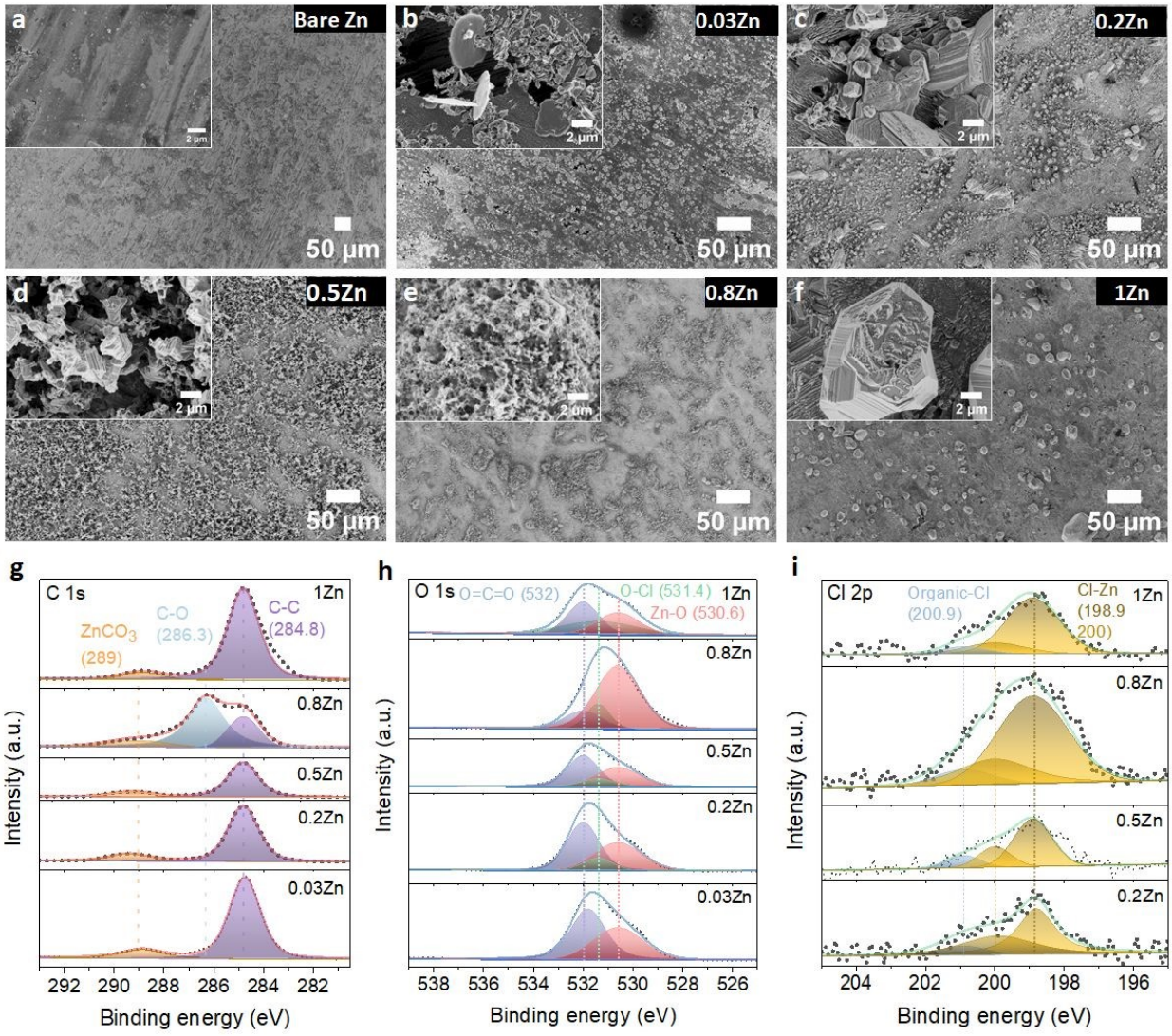

Figure 5: Morphology evolution and surface composition of Zn electrodes after 20 cycles of Zn plating/stripping in different WISEs at 1 mA cm^{-2} and 0.5 mAh cm^{-2}. SEM images of (a) bare Zn and cycled Zn anode in (b) 0.03, (c) 0.2, (d) 0.5, (e) 0.8, and (f) 1Zn electrolytes. The corresponding XPS spectra of (g) C 1s, (h) O 1s, and (i) Cl 2p.

First, the morphology of the Zn anode after 20 cycles at 1mA cm^{-2} current and 0.5 mAh cm^{-2} capacity densities was invesitigated by SEM. The SEM images on Zn anode shows uneven morphology with black spots and pits in **0.03Zn** electrolyte (**Fig. 5b**), which may be due to corrosion byproduct formation. The **0.2Zn** electrotlyte (**Fig. 5c**), on the other hand, displays deposition of small particles distributed on the Zn surface while these particules are multiplicated in **0.5Zn** indicating a more porous surface **(Fig. 5d)**. The Zn surface becomes denser and compact as the Zn ratio increases in **0.8** and **1Zn** electrolytes (**Fig. 5e** and **f**). The SEM results show that

View Article Online
DOI: 10.1039/D4TA02704C

there is no direct correlation between all Zn molar ratios, particularly those below **0.5Zn**. However, the surface of Zn foil is less rough with lower surface porosity upon increasing the Zn molar ratio from **0.5Zn**. In addition, the magnified image of the electrode, in particular in the 1Zn electrolyte, reveals a more compact and denser morphology. XPS analysis were conducted to further examine the chemical composition of cycled Zn surface. The C 1s peaks (**Fig. 5g**) are deconvoluted into three components. The binding energy at 284.8 and 286.3 eV are attributed to C-C and C-O peaks, respectively, while the peak at 289 eV is assigned to CO_3. However, the peak at 286.3 eV is observed only in **0.8Zn** electrolyte, indicating the formation of more carbonate containing species. The C 1s peaks in **1Zn** electrolyte may be originated from adsorbed organic residues contamination. The O 1s spectra (**Fig. 5h**) demonstrates the presence of three components corresponding to O=C=O (532 eV), O-Cl (531.4 eV), and Zn-O (530.6 eV) in **0.2**, **0.5**, **0.8**, and **1Zn** electrolytes, indicating the existence of inorganic residues from electrolyte decomposition. For **0.03Zn** electrolyte, since there is no chlorine, only C-O and Zn-O bonds of the Zn carbonate and Zn oxides are observed. The Cl 2p spectra shows two chlorine species corresponding to inorganic and organic chlorine at 198.9 and 200.9 eV (**Fig. 5i**). Moreover, the 2p orbital of Zn is separated into two peaks (**Fig. S15**), corresponding to $2p_{3/2}$ (1021.9 eV) and $2p_{1/2}$ (1045 eV). The above result indicates the cycled Zn surface contains organic/inorganic layer, the organic species generated form acetate (Ac) decomposition while the chlorine and Zn containing inorganic species are derived from the $ZnCl_2$. Overall, the composition of each species generated from electrolyte decomposition on Zn anode surface after cycling are similar in the different electrolytes.

3.6. WIS-like dilute electrolyte

The results aboved showed that the suppression of free water in WISEs is not enough for the stability of Zn anode, instead, it is the of Zn molar ratio that plays an important role. On the other hand, the water-deficient and anion-rich solvation structure of Zn^{2+} can be also achieved in dilute electrolytes if the solvation ability of anion is higher than that of water.[15, 38] Recently, this idea was demonstrated in $Zn(Ac)_2.2H_2O$ and KAc hybrid electrolyte since the Ac anions have a stronger coordination ability to Zn^{2+} than water. Specifically, optimal CE and rate performance were

View Article Online
DOI: 10.1039/D4TA02704C

attained with a water-to-cation ratio of 10 in the $Zn_{0.2}K_{0.8}OAc_{1.2}$ $10H_2O$ electrolyte (abbreviated here as $0.2Zn.10H_2O$).[15] To validate this concept within our prepared WISEs $[(ZnCl_2)_x(LiAc)_{1-x}/(H_2O)_n]$, we chose the **0.5Zn** electrolyte because it contains a high amount of Ac anion and considered the optimal ratio for improving CE and rate performance.

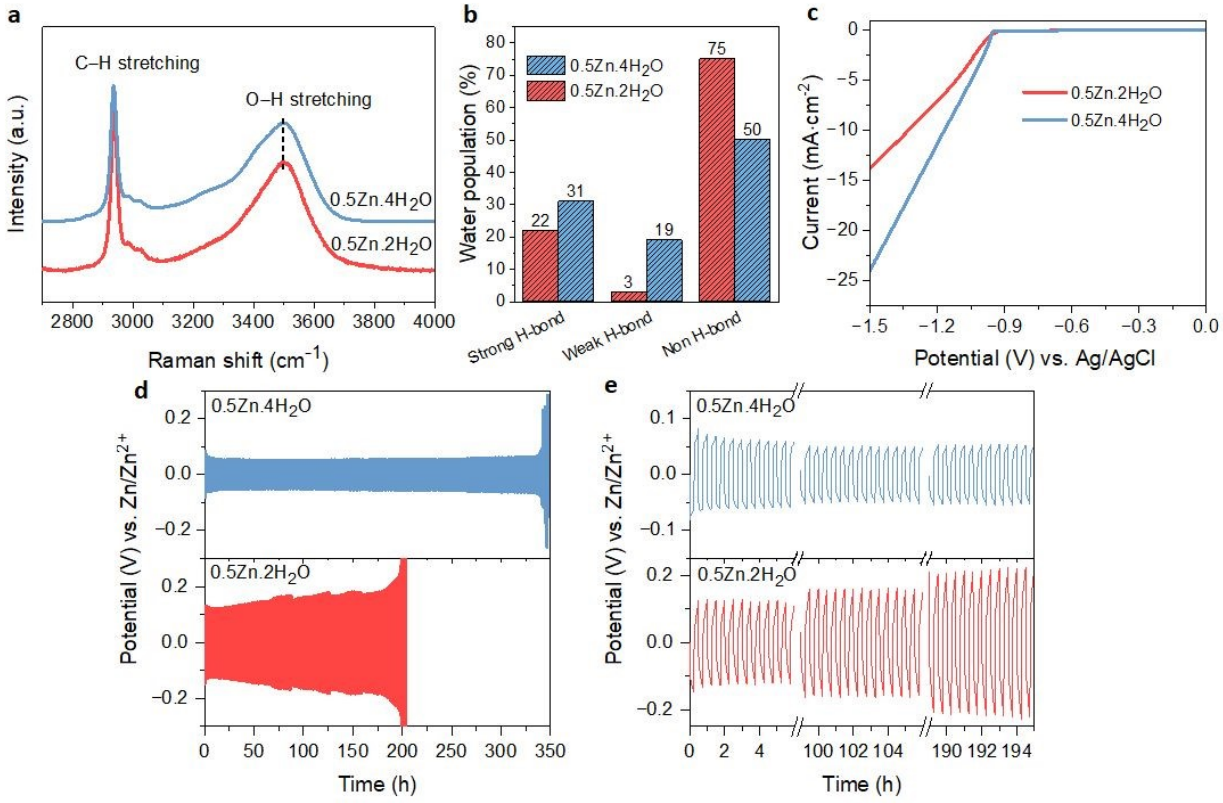

Figure 6: Solvation structure and electrochemichal stability of Zn anode in $0.5Zn.4H_2O$ electrolyte compared to concentrated $0.5Zn.2H_2O$. (a) Raman spectra in the water region. (b) The corresponding water population percentages. (c) LSV curves on Ti substrate (d) Zn plating/stripping at 2 mA cm^{-2} and 0.5 mAh cm^{-2} in Zn‖Zn symmetric cells. and (e) The corresponding potential profiles.

The **0.5Zn** (labeld as $0.5Zn.2H_2O$ herein after) WISE was diluted to 15 m by increasing the water-to-cation ratio (n) to 4 (labeled as $0.5Zn.4H_2O$). Raman spectroscopy was employed to investigate the H-bonding enviroments of water in the $0.5Zn.4H_2O$ electrolyte and compared with that of $0.5Zn.2H_2O$. As shown in **Fig. 6a**, the Raman spectra of the $0.5Zn.4H_2O$ electrolyte displayes broader peaks compared to the $0.5Zn.2H_2O$, indicating a higher concentration of water molecules relative to Ac anions. Furthermore, the deconvoluted spectra of the $0.5Zn.4H_2O$ compared to $0.5Zn.2H_2O$ electrolytes reveales distinct hydrogen-bonding environments in the water region.

View Article Online
DOI: 10.1039/D4TA02704C

As shown in **Fig. 6b** and **Fig. S16a**, the area under the sub-band associated with strongly hydrogen-bonded water molecules in the $0.5Zn.4H_2O$ electrolyte (31%) is slightly higher compared to that of the $0.5Zn.2H_2O$ electrolyte (22%). Notably, the corresponding peak position exhibites a slight shift towards lower frequencies in the $0.5Zn.4H_2O$ electrolyte (3255 cm^{-1}) compared to the $0.5Zn.2H_2O$ (3285 cm^{-1}) (**Fig. S16b**). In addition, the weak hydrogen-bond peak area increased from 3% to 19% in the diluted $0.5Zn.4H_2O$ electrolyte. The peak area attributed to non-hydrogen-bonded water is 54% in $0.5Zn.4H_2O$, which decreased in comparison to $0.5Zn.2H_2O$ electrolyte. Thus, the higher proportion of strongly hydrogen-bonded water molecules and lower proportion of non-hydrogen-bonded water in $0.5Zn.4H_2O$ compared to $0.5Zn.2H_2O$ suggests the presence of free water molecules.

The influence of free water molecules on Zn surface morphology and corrosion byproducts was investigated following immersion test in the $0.5Zn.4H_2O$ electrolyte for 10 days. Subsequent analysis using XRD techniques reveales no XRD patterns indicative of corrosion byproducts (**Fig. S17a**). However, The SEM images show many black spots and mossy particles (**Fig. S17b**), suggesting the formation of byproducts formation due to the presence of free water molecules. The CV analysis of Zn plating/stripping on Ti foil in $0.5Zn.4H_2O$ electrolyte exhibits comparable profiles to those observed in the $0.5Zn.2H_2O$ electrolyte (**Fig. S18a**), suggesting the absence of new electrochemical reactions. However, the cell utilizing $0.5Zn.4H_2O$ shows higher nucleation overpotential (14 mV) compared to that of $0.5Zn.2H_2O$. The corresponding LSV curve (**Fig. 6c**) demonstrates a notably higher cathodic current in $0.5Zn.4H_2O$ electrolyte compared to the $0.5Zn.2H_2O$ electrolyte, confirming the contribution of H_2 evolution in $0.5Zn.4H_2O$ electrolyte.

Furthermore, the effect of free water molecules in $0.5Zn.4H_2O$ electrolyte on the nucleation and growth process of Zn were investigated through CA using Zn‖Zn symmetric cells similar to the previous protocol (**Fig. S18b**). The Zn anode in $0.5Zn.4H_2O$ electrolyte shows a 2D diffusion process for 19 s longer than in $0.5Zn.2H_2O$, followed by a constant 3D diffusion process thereafter. However, the corresponding SEM images in **Fig. S18d** displays similar size and morphology as the particles in concentrated $0.5Zn.2H_2O$ – indicating similar growth mechanism. Furthermore, the $t_{Zn^{2+}}$ in $0.5Zn.4H_2O$ electrolyte is 0.54 (**Fig. S18c**), which is higher than in

View Article Online
DOI: 10.1039/D4TA02704C

0.5Zn.2H_2O electrolyte due to lower viscosity combined with increased ionic conductivity (**Table S1**).

The Zn anode plating/stripping reversibility in 0.5Zn.4H_2O electrolyte was demonstrated using Zn‖Zn half-cell at different current density with a fixed capacity of 0.5 mA cm^{-2}, as demonstrated in **Fig. 6d-e** and **Fig. S19**. The cell utilizing the 0.5Zn.4H_2O electrolyte failed after 130 cycles at lower current density of 1 mA cm^{-2}, whereas the cell with the 0.5Zn.2H_2O electrolyte sustain for 300 cycles (**Fig. S19a** and **b**). In contrast, the cell with the 0.5Zn.4H_2O electrolyte at 2 mA cm^{-2} current density sustains over 350 cycles without experiencing potential fluctuations, whereas the cell using 0.5Zn.2H_2O electrolytes experienced short circuits around 200 cycles (**Fig. 6d** and **e**). These results demonstrate that the 0.5Zn.4H_2O electrolyte offers superior Zn stability at higher current densities, while the reverse is observed at lower current densities, consistent with the LSV data in **Fig. 6c**.

The diluted electrolyte was also compared to the recently reported WIS-like $Zn_{0.2}K_{0.8}OAc_{1.2}$ 10H_2O electrolyte (abbreviated as 0.2Zn.10H_2O).[15] As depicted in **Fig. S19c** and **d**, the Zn‖Zn cell with the 0.2Zn.10H_2O electrolyte cycled for over 150 cycles with significant potential fluctuations at 1 mA cm^{-2} and 0.5 mAh cm^{-2}, while the 0.5Zn.4H_2O electrolyte provides 130 cycles but without any potential fluctuation. Doubling the current density with the same capacity yields approximately 160 cycles in the 0.2Zn.10H_2O electrolyte with higher overpotential. However, the 0.5Zn.4H_2O electrolyte deliver over 350 cycles without any potential fluctuation compared to the 0.2Zn.10H_2O electrolyte. Again these results indicates the importance for Zn molar ratio for Zn cycling stability in particular at high current density. Note, the obtained stability of 0.2Zn.10H_2O is different in this work from the reported paper. This can be explained by the difference in the Zn anode size, where here we used 13 mm in contrast to 6 mm diameter. As the Zn electrode size decreases, better contact between electrodes results from increased pressure. This heightened pressure, in turn, influences the ion flux and distribution of current. Hence, the homogoneisation of the Zn anode size is important for future research.

Finally, the cycled Zn electrodes after 20 cycles at 1 mA cm^{-2} and 0.5 mAh cm^{-2} were analysed using SEM and XPS. The SEM image illustrates a similar morphology to the Zn electrode in 0.5Zn.2H_2O electrolyte (**Fig. 5d**). However, the Zn electrode in the 0.5Zn.4H_2O electrolyte displays

View Article Online
DOI: 10.1039/D4TA02704C

a more porous and non-uniform structure (**Fig. S20**), indicative of dendrite growth and byproduct formation likely caused by the presence of free water molecules. The composition of the cycled Zn electrode was further analyzed by XPS. As shown in **Fig. S21a**, the survey spectra indicate the presence of C, O, Zn, and Cl elements. The presence of characteristic C 1s peaks at 284 eV (C-C) and 289 eV (CO_3) in **Fig. S21b** suggests the adsorption or decomposition of Ac anios on the surface of the Zn electrode. The O 1s spectra reveal the presence of C-O and C-Cl species (**Fig. S21c**), while the Cl 2p (**Fig. S21d**) exhibit organic and inorganic chlorine species. The type and position of each peak in this electrolyte are consistent with those observed in the 0.5Zn.2H_2O electrolyte discussed previously. The organic species may originate from Ac, while the inorganic species may be derived from $ZnCl_2$. Therefore, these findings indicate that optimizing the mixing salt ratio in dilute solutions also enhance Zn anode stability, particularly at higher current densities, if WIS-like coordination of Zn^{2+} ions is achieved.

4. Conclusion

In summary, we conducted a systematic investigation into how varying Zn molar ratios affect the nucleation behavior, deposition process, and cycling stability of Zn metal anodes across different WISEs. Our findings reveal a direct correlation between Zn overpotentials, deposition process, and cycling stability with the concentration of Zn^{2+} in the electrolyte. With increasing Zn molar ratio, there is an expansion in the potential difference between Zn reduction and H_2 evolution due to the positive shift in Zn reduction potential. Moreover, we observed the formation of interconnected, larger and dense Zn nuclei on Zn foil at Zn molar ratio. This phenomenon can be attributed to lower nucleation and growth overpotentials resulting from increased nucleation sites with rising Zn^{2+} concentration. Consequently, Zn metal anodes perform better in 0.5, 0.8, and 1Zn WISEs compared to 0.03 and 0.2Zn WISEs, owing to enhanced t_{Zn}^{2+} and lower overpotentials. Cycling stability analysis indicates an optimal Zn molar ratio around 0.5. Beyond the later ratio, the impact of Zn molar ratio primarily affects only Zn plating/stripping overpotentials while maintaining similar cycling times. Furthermore, taking the 0.5Zn electrolyte, the impact of water content was studied by diluting the solution by half. For the examined diluted electrolyte (0.5Zn.4H_2O), a WISE-like coordination environment is achieved around Zn^{2+}, enabling

View Article Online
DOI: 10.1039/D4TA02704C

to achieve high rate performance compared to most other concentrated electrolytes. However, to the expense of lower stability at low current density due to promoted H_2 evolution as a result of increased free water population. Hence, this study shows the importance of increasing the Zn salt concentration during the preparation of WISEs. An optimum Zn molar ratio of 0.5 was found which is already considered high in comparison to most reported WISEs in the literature. Hence, this study brings a new insight for the future design of WISEs to achieve high performant AZIBs.

Declaration of interests

The authors declare no competing interests.

Data availability

The data supporting this article have been included as part of the Supplementary Information.

Acknowledgements

This work is supported by the Max Planck Society. F.W.F. acknowledges the Alexander von Humboldt Stiftung for financial support. R.B. acknowledge funding by the European Union's Framework Program for Research and Innovation Horizon 2020(2014-2021) under the Marie Skłodowska-Curie Grant Agreement No. 101032227.

References

1. *Y. Zou, X. Yang, L. Shen, Y. Su, Z. Chen, X. Gao, J. Zhou and J. Sun, Energy Environ. Sci., 2022, **15**, 5017-5038.*
2. *J. Cao, D. Zhang, X. Zhang, Z. Zeng, J. Qin and Y. Huang, Energy Environ. Sci., 2022, **15**, 499-528.*
3. *Z. Li and A. W. Robertson, Battery Energy, 2022, **2**, 1-30.*
4. *W. Yang, Y. Yang, H. Yang and H. Zhou, ACS Energy Lett., 2022, **7**, 2515-2530.*
5. *L. Cao, D. Li, T. Deng, Q. Li and C. Wang, Angew. Chem., Int. Ed., 2020, **59**, 19292-19296.*
6. *O. O. Sofronov and H. J. Bakker, ACS Cent. Sci., 2020, **6**, 1150-1158.*
7. *C. Liu, X. Xie, B. Lu, J. Zhou and S. Liang, ACS Energy Lett., 2021, **6**, 1015-1033.*
8. *V. Verma, S. Kumar, W. Manalastas and M. Srinivasan, ACS Energy Lett., 2021, **6**, 1773-1785.*
9. *F. Wang, O. Borodin, T. Gao, X. Fan, W. Sun, F. Han, A. Faraone, J. A. Dura, K. Xu and C. Wang, Nat. Mater., 2018, **17**, 543-549.*
10. *C. Zhang, J. Holoubek, X. Wu, A. Daniyar, L. Zhu, C. Chen, D. P. Leonard, I. A. Rodriguez-Perez, J. X. Jiang, C. Fang and X. Ji, Chem. Commun., 2018, **54**, 14097-14099.*
11. *F. Yang, J. A. Yuwono, J. Hao, J. Long, L. Yuan, Y. Wang, S. Liu, Y. Fan, S. Zhao and K. Davey, Adv. Mater., 2022, **34**, 2206754-2206766.*
12. *S. Chen, R. Lan, J. Humphreys and S. Tao, Energy Storage Mater., 2020, **28**, 205-215.*
13. *Y. Zhu, J. Yin, X. Zheng, A.-H. Emwas, Y. Lei, O. F. Mohammed, Y. Cui and H. N. Alshareef, Energy Environ. Sci., 2021, **14**, 4463-4473.*

View Article Online
DOI: 10.1039/D4TA02704C

14. R. Bouchal, I. Al Kathemi and M. Antonietti, Small, 2023, 2309556-2309567.
15. D. Gomez Vazquez, T. P. Pollard, J. Mars, J. M. Yoo, H.-G. Steinrück, S. E. Bone, O. V. Safonova, M. F. Toney, O. Borodin and M. R. Lukatskaya, Energy Environ. Sci., 2023, **16**, 1982-1991.
16. I. Bodachivskyi, U. Kuzhiumparambil and D. B. G. Williams, Catalysis Science & Technology, 2019, **9**, 4693-4701.
17. D. E. Irish, B. McCarroll and T. F. Young, The Journal of Chemical Physics, 1963, **39**, 3436-3444.
18. X. Guo and G. He, Journal of Materials Chemistry A, 2023, **11**, 11987-12001.
19. D. Dong, T. Wang, Y. Sun, J. Fan and Y.-C. Lu, Nat. Sustain., 2023, 1674-1484.
20. D. Mendes de Oliveira, S. R. Zukowski, V. Palivec, J. Henin, H. Martinez-Seara, D. Ben-Amotz, P. Jungwirth and E. Duboue-Dijon, Phys. Chem. Chem. Phys., 2020, **22**, 24014-24027.
21. C. Li, S. Jin, L. A. Archer and L. F. Nazar, Joule, 2022, **6**, 1733-1738.
22. H. Jiang, L. Tang, Y. Fu, S. Wang, S. K. Sandstrom, A. M. Scida, G. Li, D. Hoang, J. J. Hong, N.-C. Chiu, K. C. Stylianou, W. F. Stickle, D. Wang, J. Li, P. A. Greaney, C. Fang and X. Ji, Nat. Sustain., 2023, **6**, 806-815.
23. Y. Wang, T. Wang, S. Bu, J. Zhu, Y. Wang, R. Zhang, H. Hong, W. Zhang, J. Fan and C. Zhi, Nat. Commun., 2023, **14**, 1828-1841.
24. B. Gavriel, N. Shpigel, F. Malchik, G. Bergman, M. Turgeman, M. D. Levi and D. Aurbach, Energy Storage Materials, 2021, **38**, 535-541.
25. M. Amiri and D. Bélanger, ChemElectroChem, 2021, **8**, 2737-2745.
26. F. Yang, J. A. Yuwono, J. Hao, J. Long, L. Yuan, Y. Wang, S. Liu, Y. Fan, S. Zhao, K. Davey and Z. Guo, Adv. Mater., 2022, **34**, 2206754-2206766.
27. Z. Zhao, J. Zhao, Z. Hu, J. Li, J. Li, Y. Zhang, C. Wang and G. Cui, Energy Environ. Sci., 2019, **12**, 1938-1949.
28. H. Liu, Y. Zhang, C. Wang, J. N. Glazer, Z. Shan and N. Liu, ACS Appl. Mater. Interfaces, 2021, **13**, 32930-32936.
29. J. Wan, R. Wang, Z. Liu, S. Zhang, J. Hao, J. Mao, H. Li, D. Chao, L. Zhang and C. Zhang, Adv. Mater., 2024, **36**, 2310623-2310636.
30. Q. Zou, Z. Liang, W. Wang, D. Dong and Y.-C. Lu, Energy Environ. Sci., 2023, **16**, 6026-6034.
31. A. Pei, G. Zheng, F. Shi, Y. Li and Y. Cui, Nano Lett., 2017, **17**, 1132-1139.
32. K. Yan, J. Wang, S. Zhao, D. Zhou, B. Sun, Y. Cui and G. Wang, Angew. Chem., Int. Ed. , 2019, **58**, 11364-11368.
33. Y. Zhao, S. Guo, M. Chen, B. Lu, X. Zhang, S. Liang and J. Zhou, Nat. Commun., 2023, **14**, 7080-7091.
34. H. Peng, C. Liu, N. Wang, C. Wang, D. Wang, Y. Li, B. Chen, J. Yang and Y. Qian, Energy Environ. Sci., 2022, **15**, 1682-1693.
35. D. Han, C. Cui, K. Zhang, Z. Wang, J. Gao, Y. Guo, Z. Zhang, S. Wu, L. Yin, Z. Weng, F. Kang and Q.-H. Yang, Nat. Sustain., 2021, **5**, 205-213.
36. L. Cao, D. Li, T. Pollard, T. Deng, B. Zhang, C. Yang, L. Chen, J. Vatamanu, E. Hu, M. J. Hourwitz, L. Ma, M. Ding, Q. Li, S. Hou, K. Gaskell, J. T. Fourkas, X. Q. Yang, K. Xu, O. Borodin and C. Wang, Nat. Nanotechnol., 2021, **16**, 902-910.
37. Y. Deng, H. Wang, M. Fan, B. Zhan, L. J. Zuo, C. Chen and L. Yan, J. Am. Chem. Soc., 2023, **145**, 20109-20120.
38. S. Alvarez, Chem. Eur. J., 2020, **26**, 4350-4377.

View Article Online
DOI: 10.1039/D4TA02704C

Data availability

The data supporting this article have been included as part of the Supplementary Information.